

Estimating and Correcting the Device-Under-Test Transfer Function in Loaded Reverberation Chambers for Over-the-Air Tests

Kate A. Remley, *Fellow, IEEE*, Ryan J. Pirkel, *Member, IEEE*, Chih-Ming Wang, Damir Senić, *Member, IEEE*, Arvand C. Homer, Matt V. North, Maria G. Becker, Robert D. Horansky, *Member, IEEE*, and Christopher L. Holloway, *Fellow, IEEE*

Abstract—We assess the potential error in measurements of the power transfer function corresponding to a reverberation chamber set-up when different antenna types are used for the reference and device-under-test measurements. We derive a mathematical description of the transfer function that accounts for differences in the amount of unstirred energy, represented by the spatially averaged K factor, arising from various antenna types. Our results show that loaded chamber configurations, combined with reference/device antenna pairs having significantly different radiation patterns, can result in statistically significant errors in the prediction of the transfer function. If it is possible to obtain an estimate of the K factor associated with the device antenna, this correction can improve the estimate of the transfer function that would be experienced by the device under test. Finally, we develop a method that could be used in standardized test methods to bound the uncertainty associated with the unknown K factor for common antenna types.

Index Terms—Antenna radiation pattern, cellular telecommunications, microwave measurement, over-the-air (OTA) test, reverberation chamber, Rician K factor, wireless system.

I. INTRODUCTION

REVERBERATION chambers are becoming a popular test facility for over-the-air (OTA) testing of wireless devices such as smartphones, cellular-enabled machine-to-machine or

Internet-of-Things equipment, and other such systems [1]–[5]. One key difference between “traditional” reverberation chamber measurements of devices with continuous-wave signals and those in which communications signals must be demodulated is the need for loading the chamber with RF absorber to broaden the coherence bandwidth [6]–[8]. Such loading provides a channel with fading characteristics [9] similar to that for which the device was designed to operate. Essentially, the reverberation-chamber cavity acts as a bandpass filter, with higher Q chambers presenting a narrower passband. Loading the chamber reduces Q , increases the passband, and facilitates the undistorted demodulation of the received communication signal. A common rule of thumb is to load the chamber such that the coherence bandwidth exceeds the bandwidth of the received signal (or independent subcarrier), although, in practice, error correction may enable the use of narrower coherence bandwidths.

Standard practice for both electromagnetic compatibility/interference measurements and OTA tests in reverberation chambers involves minimizing the “unstirred energy” corresponding to fields in the chamber that do not, on average, interact with mode-stirring mechanisms [10]–[12]. Examples of unstirred energy include wall reflections or direct transmission between antennas. In a loaded chamber, the amount of stirred energy in the chamber decreases relative to the unstirred energy because the unstirred components are unimpeded by the RF absorber. If not properly accounted for, unstirred energy may result in an increase in measurement uncertainty because the measured device-under-test (DUT) response becomes position dependent and correlation between mode-stirring samples may increase [13], [14]. This has motivated the use of platform and antenna polarization stirring, in addition to the use of mechanical mode-stirrers, for loaded chambers [13]–[15].

The placement and orientation of the antennas with respect to the chamber walls, mechanical mode stirrers, other antennas, and RF absorber can also be optimized to reduce the unstirred energy. However, when the antenna radiation pattern is unknown, as it may be for a DUT with an integrated antenna, use of these techniques may be difficult. The present work explores the impact on the estimate of the chamber’s transfer function (*i.e.*, chamber loss) when the antenna characteristics are unknown, and provides a correction factor when the user has access to the DUT’s antenna terminals.

Manuscript received April 30, 2017; accepted May 15, 2017. Date of publication June 16, 2017; date of current version August 17, 2017. Publication of the United States government, not subject to copyright in USA. (*Corresponding author: Kate A. Remley.*)

K. A. Remley, D. Senić, M. V. North, M. G. Becker, R. D. Horansky and C. L. Holloway are with the Communications Technology Laboratory, National Institute of Standards and Technology, Boulder, CO 80305 USA (e-mail: kate.remley@nist.gov; damir.senic@nist.gov; matt.north@nist.gov; maria.becker@nist.gov; robert.horansky@nist.gov; holloway@boulder.nist.gov).

R. J. Pirkel was a National Research Council Post doctoral Research Associate at NIST. He is now with the Signal and Information Sciences Laboratory University of Texas Applied Research Laboratory, Austin, TX USA (e-mail: rpirkel@gmail.com).

C.-M. Wang is with the Statistical Engineering Division, National Institute of Standards and Technology, Boulder, CO 80305 USA (e-mail: chih-ming.wang@nist.gov).

A. C. Homer was a Summer research fellow at the National Institute of Standards and Technology, Boulder, CO, in 2016. He is a student at the University of Maryland, College Park, MD, USA. (e-mail: arvandhomer@verizon.net).

Color versions of one or more of the figures in this paper are available online at <http://ieeexplore.ieee.org>.

Digital Object Identifier 10.1109/TEM.2017.2708985

In an ideal, unloaded chamber, the radiation pattern of any antenna is effectively isotropic [16]. However, in loaded chambers, the radiation pattern of the antenna may affect the measured result. This is explained as follows: energy that radiates out of the transmit antenna will spread in various directions. The amount of energy that is absorbed before it reaches the receive antenna depends on several factors including the antenna type and pattern, the position and orientation of the antenna with respect to the absorber, as well as the electrical surface area (a function of both frequency and physical size) of the absorber exposed to the antenna. One example of this was discussed in [17], where we showed that when an antenna is in close proximity to, or oriented toward, RF absorber, estimates of the chamber set-up's Q and the received power varied. Test procedures were developed to ensure that antennas are placed sufficiently far from the absorbing material [5], [18], minimizing the so-called proximity effect on the reference power transfer function. However, as discussed below, in some cases, it is not only the close-proximity effects that may affect the measured estimate of the transfer function.

It is crucial to understand the severity of this effect because the reference measurement, which provides an estimate of the chamber loss experienced by the DUT, typically involves a different antenna than that of the DUT. An error in the estimate of the chamber transfer function will affect the accuracy of metrics intended to quantify DUT performance such as total radiated power (TRP) or total isotropic sensitivity (TIS). Current practice [5], [8], [13] consists of using an antenna for the reference measurement with a radiation pattern that is “similar” to that of the DUT. As stated above, it is not always possible to know the characteristics of the DUT antenna. An estimate of the additional uncertainty, if any, introduced by this “unknown K factor” is desirable.

In the present work, we explore the significance of the unknown K factor on the estimate of the chamber set-up's power transfer function. As we will show, in many cases, the error made by estimating the transfer function G_{DUT} experienced by the DUT directly from the reference power transfer function G_{Ref} is not statistically significant. However, for cases where it is significant, we develop a method by which the reference power transfer function may be improved by accounting for the difference in the K factors introduced by the reference and DUT antennas. If we have an estimate of the K factor for the DUT antenna set-up, this correction can significantly improve the estimate of the transfer function that would be experienced by the DUT for some configurations.

In Section II, we describe one commonly used approach to characterize the reference power transfer function for a reverberation-chamber set-up. We then extend this work to account for the K factor associated with the reference and DUT antennas, leading to an improved estimate of the chamber's power transfer function, as seen by the DUT. In Section III, we present measurements of several reverberation-chamber configurations with antennas that introduce various K factor values. These measurements, made under several different loading conditions, utilized antennas for which we could directly assess the K factor. This allows us to estimate the error arising from the assumption that the radiation patterns of

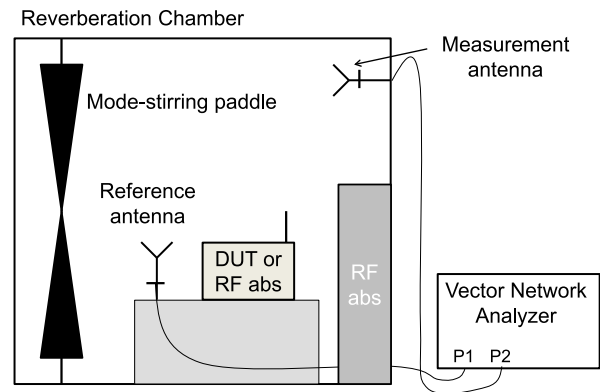


Fig. 1. Configuration for measuring the reference power transfer function for a cellular wireless device (from [5]). The chamber is loaded with RF absorber (“RF abs”) to broaden the coherence bandwidth. The reference antenna undergoes the same stirring sequence as the device under test. The measurement reference planes are denoted by perpendicular lines at the base of each antenna.

the reference and DUT antennas are “similar,” when actually they are not. We then illustrate cases where the correction factor derived in Section II can reduce this error and discuss why. In Section IV, we propose methods to estimate an upper bound on uncertainty for various antenna types and discuss the applicability of the procedures outlined here for OTA test of wireless devices. Finally, Section V concludes the paper.

II. POWER TRANSFER FUNCTION AND THE K FACTOR

A. Estimating the Chamber Set-Up's Power Transfer Function

Well-established procedures for estimating power-based metrics such as TRP and TIS from reverberation-chamber measurements require removing the power loss associated with the chamber itself as well as the losses and mismatch associated with the transmit and receive antennas [5], [8], [13], [19]. This is illustrated in Fig. 1, which shows a common set-up for cellular device testing in which the reference antenna, used to estimate the chamber loss for the DUT measurement, undergoes the same stirring sequence as the DUT. Such an estimate can be quite accurate (as we show in Section III) for both unloaded chamber set-ups and for loaded chambers, if for the latter, the reference antenna and DUT have similar radiation characteristics.

For the configuration shown in Fig. 1, the “Measurement antenna” is the receive antenna for the reference measurement and for TRP measurements. The “Reference antenna” is the transmit antenna for the reference measurement. The DUT antenna may be connectorized or integrated into the body of the wireless device to be tested. The rotating platform is used to minimize the effects of the reduced spatial uniformity of the averaged fields within the chamber caused by loading. “RF abs” refers to the RF absorber used to broaden the coherence bandwidth for demodulation of the received signal.

To obtain the chamber set-up's power transfer function, S -parameter measurements are made with the vector network analyzer (VNA) at the reference planes at the base of each antenna of Fig. 1. This measurement involves a cascade of the two antennas plus the chamber loss. In postprocessing, the antennas are

de-embedded (in terms of both mismatch and efficiency) and the ensemble average is taken over the samples acquired during the mode-stirring sequence. The result is an estimate of the reference power transfer function G_{Ref} . G_{Ref} is intended to provide an estimate of the actual power transfer function that would be experienced by the DUT G_{DUT} when power-based metrics such as TRP (given by P_{TRP}) or TIS (given by P_{TIS}) are computed. Note that we define G_{Ref} and G_{DUT} as gains so that a reduction in power is denoted with a decrease in their value.

To derive G_{Ref} from measurement, we take the average of measurements made over a mode-stirring sequence. In the present work, we define a stirring sequence as a set of unique, static conditions within the chamber provided by various stepped combinations of mode-stirring mechanisms including mechanical paddle orientations, antenna positions, and antenna orientations. In our work, the measurement data acquired *within* a stirring sequence consist of N_W stepped mode-stirring samples. The value of G_{Ref} , estimated from a *single* realization of a given stirring sequence, may be computed from VNA measurements [5], [13], [19]:

$$G_{\text{Ref}} \approx \langle G_R \rangle_{N_W} \equiv \frac{\langle |S_{21,\text{Ref}}|^2 \rangle_{N_F N_W}}{(1 - |\Gamma_M|^2) \eta_M (1 - |\Gamma_R|^2) \eta_R}, \quad (1)$$

where the ensemble average, denoted by $\langle \cdot \rangle$, of the magnitude-squared of the transmission parameter $|S_{21,\text{Ref}}|^2$ is carried out at N_F frequencies for N_W stepped mode-stirring samples. For OTA tests, the measurement bandwidth typically corresponds to the bandwidth of the communications channel. Γ_M and Γ_R correspond to the free-space reflection coefficients of the antennas. We assume that the ensemble average of the measured reflection parameters corresponds to the free-space reflection coefficient, that is, $\langle S_{jj,X} \rangle \cong \Gamma_X$, where $j = 1, 2$ and $X = R, M$. The reader is referred to [19, Appendix A] for more information on the derivation of (1). In (1), η_M and η_R are the radiation efficiencies of the measurement and reference antennas, respectively. They may be found from manufacturer's specifications, or from measurements made in an anechoic or unloaded reverberation chamber [20]. Note that some derivations refer to the product $(1 - |\Gamma_X|^2) \eta_X$ as "total efficiency."

Once G_{Ref} has been estimated for a given chamber set-up, the total power radiated by the DUT, the TRP (P_{TRP}) or TIS (P_{TIS}) may be estimated as follows:

$$P_{\text{TRP}} = \frac{\langle P_{\text{Meas}} \rangle_{N_W} |1 - \Gamma_M \Gamma_{\text{RX}}|^2}{G_{\text{Ref}} (1 - |\Gamma_M|^2) \eta_M} \quad (2)$$

or

$$P_{\text{TIS}} = \frac{G_{\text{Ref}} (1 - |\Gamma_M|^2) \eta_M |1 - \Gamma_M \Gamma_{\text{RX}}|^2}{\langle P_{\text{Meas}} \rangle_{N_W}} \quad (3)$$

where $\langle P_{\text{Meas}} \rangle_{N_W}$ is the ensemble average over N_W stepped mode-stirring samples in the frequency band of interest. For TRP, each sample P_{Meas,n_W} is typically acquired by a base-station-emulator, spectrum analyzer, or other power-calibrated instrument. For each TIS measurement sample, the output power

P_{Meas,n_W} is decreased on the base station emulator until a specified bit error/block error level is reached on the device under test. The free-space reflection coefficient of the reference antenna is $\langle S_{11}^R \rangle \cong \Gamma_R$. The term Γ_{RX} is the reflection coefficient of the base-station emulator or spectrum analyzer receiver assembly (including cable, if used), typically measured with a VNA. Refer to [19] for additional information.

B. Uncertainty in the Estimate of G_{Ref}

In current standardized test procedures [3], [5], uncertainty in the estimate of G_{Ref} is found *between* N_B realizations of a particular stirring sequence implemented within the chamber. This is because the lack of spatial uniformity of the averaged fields in the chamber is often the dominant component of uncertainty in loaded-chamber measurements [19]. In many cases, these $N_B = 9$ measurements are made at b_j , $j = 1 \dots N_B$ spatially uncorrelated locations within the chamber and the uncertainty is given by [19]

$$u_{\text{Ref}}^2 = \frac{1}{N_B(N_B - 1)} \sum_{j=1}^{N_B} \left(\langle G_R(b_j) \rangle_{N_W} - \hat{G}_{\text{Ref}} \right)^2 \quad (4)$$

where \hat{G}_{Ref} is the mean of the $N_B = 9$ measurements.

The standard deviation of these nine measurements, $\sigma_{G_{\text{Ref}}} = \sqrt{N_B} u_{\text{Ref}}$, is often used as a metric to assess the lack of spatial uniformity for the particular chamber set-up [5], [8], [13]. Its value is provided below during our chamber assessment.

To find, for example, the expanded uncertainty U_{95} corresponding to a 95% confidence level, the coverage factor k_{95} is determined from the degrees of freedom corresponding to u_{Ref}^2 . The number of degrees of freedom is then used to calculate the coverage factor k_{95} as recommended in [21, Appendix B3]. That is, $k_{95} = t_{95}(v)$, where $t_{95}(v)$ is the two-sided 95th percentile of the Student's t -distribution having v degrees of freedom.

The expanded uncertainty is given by [19]

$$U_{95,\text{Ref}} = k_{95} u_{\text{Ref}} = \frac{k_{95} \sigma_{G_{\text{Ref}}}}{\sqrt{N_B}}, \quad (5)$$

where k is the coverage factor. Based on $N_B = 9$ measurements, the value of k for various confidence levels is presented in Table I [21]. These values will be used in the following sections to assess the significance of errors in estimating G_{DUT} from G_{Ref} due to the unknown K factor of the DUT antenna.

TABLE I
COVERAGE FACTOR FOR VARIOUS CONFIDENCE LEVELS FOR NINE
INDEPENDENT SAMPLES (EIGHT DEGREES OF FREEDOM)

Confidence Level (%)	Coverage Factor, k
90	1.86
95	2.31
99	3.36

C. Including the K Factor to Improve the Estimate of G_{DUT}

In wireless communications channels, the Rician K factor is a metric that characterizes the ratio of direct-plus-strong-discrete multipath components to diffuse scattering [9]. The Rician K factor (or simply “ K factor”) associated with a given reverberation-chamber set-up is typically computed by separating out and then averaging the unstirred and stirred components that were acquired over a complete mode-stirring sequence, and then forming their ratio [22], [23]. Such measurements are typically made with a vector network analyzer, rather than the DUT itself because it is difficult to accurately obtain the stirred and unstirred components without directional couplers and access to the antenna ports. Also, performing impedance mismatch correction is trivial for VNA-measured quantities.

Equations (1) and (2) assume that the power transfer function presented by the chamber set-up does not change between the reference and DUT measurements; that is, that $G_{\text{Ref}} = G_{\text{DUT}}$. To better understand the effect on the transfer function arising from the use of different antenna types for the reference and DUT measurements, we may decompose the chamber’s complex and implicitly frequency-dependent *linear* (as opposed to *power*) transfer function T_{R} into stirred T_{R}^{s} and unstirred T_{R}^{u} components, where for each of the w_i stepped mode-stirring samples (where $i = 1 \dots N_W$), we have

$$T_{\text{R}}(w_i, \text{pos}, w_i, \text{env}) = T_{\text{R}}^{\text{u}}(w_i, \text{pos}) + T_{\text{R}}^{\text{s}}(w_i, \text{pos}, w_i, \text{env}) \quad (6)$$

where $G_{\text{Ref}} = \langle |T_{\text{R}}|^2 \rangle_{N_W}$ is the total number of stepped mode-stirring samples within a mode-stirring sequence. The variable w_i, pos represents those mode-stirring samples that are a function of antenna position and/or polarization; that is, those that are a function of the reference antenna, measurement antenna, or DUT position within the chamber environment. The variable w_i, env represents those samples that are a function of mechanical paddle position, that is, those stirring mechanisms related to a changing environment within the chamber [14]. This distinction is necessary because the unstirred component represents energy that is not affected by the changing environment (*e.g.*, does not interact with the paddle) and, thus, for a single antenna position is not a function of w_i, env .

We convert the linear transfer function into power-like quantities and take the ensemble average over all mode-stirring samples as in (1):

$$\langle G_{\text{R}}(w_i, \text{pos}, w_i, \text{env}) \rangle = \langle |T_{\text{R}}^{\text{u}}(w_i, \text{pos}) + T_{\text{R}}^{\text{s}}(w_i, \text{pos}, w_i, \text{env})|^2 \rangle \quad (7a)$$

$$\begin{aligned} &= \langle |T_{\text{R}}^{\text{u}}(w_i, \text{pos})|^2 |T_{\text{R}}^{\text{s}}(w_i, \text{pos}, w_i, \text{env})|^2 \\ &\quad \times (T_{\text{R}}^{\text{u}}(w_i, \text{pos})) (T_{\text{R}}^{\text{s}}(w_i, \text{pos}, w_i, \text{env}))^* \\ &\quad + (T_{\text{R}}^{\text{u}}(w_i, \text{pos}))^* (T_{\text{R}}^{\text{s}}(w_i, \text{pos}, w_i, \text{env})) \rangle. \quad (7b) \end{aligned}$$

The expansion in (7) may be simplified by assuming that there is no correlation between the stirred and unstirred components and that the stirred components are randomly distributed with a

zero mean, that is,

$$\lim_{w_i \rightarrow \infty} \langle T_{\text{R}}^{\text{s}}(w_i) \rangle = 0. \quad (8)$$

Then

$$\begin{aligned} \langle G_{\text{R}}(w_i, \text{pos}, w_i, \text{env}) \rangle &\approx |T_{\text{R}}^{\text{u}}(w_i, \text{pos})|^2 \\ &\quad + \langle |T_{\text{R}}^{\text{s}}(w_i, \text{pos}, w_i, \text{env})|^2 \rangle. \quad (9) \end{aligned}$$

The spatially averaged Rician K factor [22], [23] may then be given by

$$\kappa_{\text{R}} = \langle K_{\text{R}} \rangle_{N_W} = \lim_{w_i \rightarrow \infty} \frac{\langle |T_{\text{R}}^{\text{u}}(w_i, \text{pos})|^2 \rangle}{\langle |T_{\text{R}}^{\text{s}}(w_i, \text{pos}, w_i, \text{env})|^2 \rangle}, \quad (10)$$

where the ensemble average has been taken over all N_W mode-stirring positions, including paddle- and position-related samples. We can then rewrite (9) and (10) as

$$\frac{\langle G_{\text{R}}(w_i, \text{pos}, w_i, \text{env}) \rangle}{1 + \kappa_{\text{R}}} \approx \langle |T_{\text{R}}^{\text{s}}(w_i, \text{pos}, w_i, \text{env})|^2 \rangle. \quad (11)$$

Similarly, for the DUT, we have

$$\frac{\langle G_{\text{D}}(w_i, \text{pos}, w_i, \text{env}) \rangle}{1 + \kappa_{\text{D}}} \approx \langle |T_{\text{D}}^{\text{s}}(w_i, \text{pos}, w_i, \text{env})|^2 \rangle, \quad (12)$$

where we assume nominally the same N_W mode-stirring samples are used for the DUT measurement.

If the chamber is loaded identically for the reference and DUT measurements, we may assume that the mean of the magnitude-squared of the stirred chamber power transfer functions should be equal for the reference and DUT measurements:

$$\lim_{w_i \rightarrow \infty} \langle |T_{\text{R}}^{\text{s}}(w_i)|^2 \rangle = \lim_{w_i \rightarrow \infty} \langle |T_{\text{D}}^{\text{s}}(w_i)|^2 \rangle, \quad (13)$$

where the counter w_i encompasses all of the mode-stirring samples, as discussed above.

From (11) to (13), we can then show that

$$\frac{\langle G_{\text{D}} \rangle_{N_W}}{\langle G_{\text{R}} \rangle_{N_W}} \approx \frac{1 + \kappa_{\text{D}}}{1 + \kappa_{\text{R}}}. \quad (14)$$

Consequently, G_{DUT} can be estimated by use of

$$G_{\text{DUT}} = \langle G_{\text{D}} \rangle_{N_W} \approx \langle G_{\text{R}} \rangle_{N_W} \frac{1 + \kappa_{\text{D}}}{1 + \kappa_{\text{R}}}, \quad (15)$$

leading to an estimate of the chamber’s power transfer function, as experienced by the DUT, as

$$G_{\text{DUT}} = \frac{\langle |S_{21, \text{Ref}}|^2 \rangle_{N_F N_W} (1 + \kappa_{\text{D}})}{\left(1 - |\Gamma_{\text{M}}|^2\right) \eta_{\text{M}} \left(1 - |\Gamma_{\text{R}}|^2\right) \eta_{\text{R}} (1 + \kappa_{\text{R}})}. \quad (16)$$

The ratio $\frac{1 + \kappa_{\text{D}}}{1 + \kappa_{\text{R}}}$ on the right side of (15) and (16) represents a correction factor that may be used to refine the estimate of G_{DUT} when the DUT antenna introduces a different K factor from that of the reference antenna. Note that (15) requires that we obtain a sufficiently accurate estimate of the spatially averaged K factors. We may obtain an improved estimate of the wireless metrics TRP and TIS by using (16) in place of G_{Ref} in (2) and (3). As we discussed below, it may be possible to

approximately bound the correction factor for common antenna types, allowing the unknown K factor to be represented by an increase in measurement uncertainty within standardized test procedures.

III. MEASUREMENT CONFIGURATION AND CHAMBER CHARACTERIZATION

To illustrate the applicability of the correction factor of (15), we first estimate G_{Ref} and κ_{R} for several common antenna configurations. From these, we estimate G_{DUT} directly from G_{Ref} , as is current practice, or from G_{Ref} modified by the correction factor of (15) ($G_{\text{DUT, Pred}}$). Corrections that reduce the uncertainty in our estimate of G_{DUT} beyond the standard uncertainty defined below are considered significant. We illustrate measurements in cellular bands and at millimeter-wave (mmWave) frequencies, with the latter frequencies of interest for future 5G cellular wireless applications.

A. Chamber Set-Ups

For the microwave bands, we used a large reverberation chamber with interior dimensions $4.6 \text{ m} \times 3.1 \text{ m} \times 2.8 \text{ m}$, which corresponds to an electrical size of $15.3 \lambda \times 10.3 \lambda \times 9.3 \lambda$ at 1 GHz. The chamber has a single rotating mechanical mode stirrer that traces out a cylinder with a radius of approximately 0.50 m and a height of 2.10 m, see [8] and [19]. The use of a single paddle without position stirring provides less-than-optimal randomization of the measured fields within the chamber under loaded conditions. However, our goal was to utilize a scenario with higher-than-average uncertainties to understand the effectiveness of the proposed method in reducing the error involved in estimating G_{DUT} . Commercially available chamber set-ups for wireless test typically use position stirring in addition to multiple mechanical stirrers and would naturally have lower variation over the $N_B = 9$ measurements.

The chamber used for the mmWave measurements was $1.0 \text{ m} \times 0.65 \text{ m} \times 0.55 \text{ m}$, which corresponds to an electrical size of approximately $150 \lambda \times 100 \lambda \times 80 \lambda$, at the center frequency of 45 GHz. Thus, this chamber had a very large electrical size despite its small physical size. Two mechanical stirrers consisted of rotating paddles. The larger one rotated about a horizontal axis within a cylindrical volume of 0.6-m height and 0.2-m diameter, while the smaller one rotated about a vertical axis within a volume of 0.5-m height and 0.2-m diameter.

VNA measurements were conducted at the frequency bands of interest to derive estimates of G_{Ref} and κ_{R} . Measurement parameters are reported in Table II. Each measurement consisted of complex frequency data acquired by our VNA at multiple independent, stepped-paddle positions consisting of 72 for the ‘‘Cellular’’ and personal communication service (PCS) bands and 10 000 for the mmWave band. At each paddle position, frequency averaging was carried out across the band of interest (Cellular, PCS, or mmWave). These samples were then averaged over all paddle positions to obtain a single measurement; see (1) and (10).

TABLE II
VNA MEASUREMENT PARAMETERS

PARAMETER	VALUE	
Frequency	Cellular band	800–900 MHz
Range	PCS band	1.8–1.95 GHz
	mmWave band	43–47 GHz
Frequency Step, Δf	Cellular, PCS	50 kHz
	mmWave	2.5 MHz
VNA IF Bandwidth	Cellular, PCS	1 kHz
	mmWave	2 kHz
VNA Output Power Level (nominal)		–10 dBm
VNA Dwell Time		10 μs
Paddle step size	Cellular, PCS (V only)	5.0°
	mmWave ($V \times H$)	3.6° \times 3.6°
Paddle Orientations	Cellular, PCS (V only)	72
	mmWave ($V \times H$)	100 \times 100
Reference Planes	Cellular, PCS	N-type connector at antenna input ports
	mmWave	2.4 mm connectors at input to coax-to-WR-22 adapters

B. Antenna Types

For the microwave-band data reported below, the measurement (receive) antenna was a dual-ridge-horn antenna (DRHA) oriented toward the rotating paddle in the corner of the chamber, as shown in Fig. 2(a) and (c). For the mmWave-band measurements, the measurement antenna was a WR-22 waveguide horn antenna, shown at the rear of the chamber in Fig. 2(d).

Our goal was to study antenna configurations having high and low K factors. To do this, we paired the measurement antenna with one of several reference (transmit) antennas while holding the other aspects of the chamber configuration constant, including the loading, mode-stirring positions, and measurement-antenna position. We performed measurements at nine reference-antenna locations that were nominally the same for each antenna type. For the microwave bands, we located each reference antenna at three stationary positions on a rotating platform and oriented them along three orthogonal orientations, except where noted (e.g., where antennas were oriented away from each other and cross polarization was maintained). For the mmWave bands, we placed the reference antenna at nine locations. In both bands, spatial correlation, calculated with Pearson’s cross correlation formula [6], was below 0.3.

Fig. 2(a)–(d) shows the antenna configurations that we selected, with the characteristics of the various antennas provided in Table III. The ‘‘higher’’ K -factor configurations utilized azimuthally omnidirectional and omnidirectional-like reference antennas represented by a discone, shown at right in Fig. 2(a) (termed ‘‘omni’’), the antenna associated with a commercially available router, shown in Fig. 2(b) (termed ‘‘router’’), and a ‘‘randomly polarized’’ DRHA of the same type as the measurement antenna (termed ‘‘DRHA RPol’’). The randomly polarized reference DRHA was allowed to vary in its angle and position of orientation with respect to the measurement antenna. The back lobe of this DRHA is quite high and the

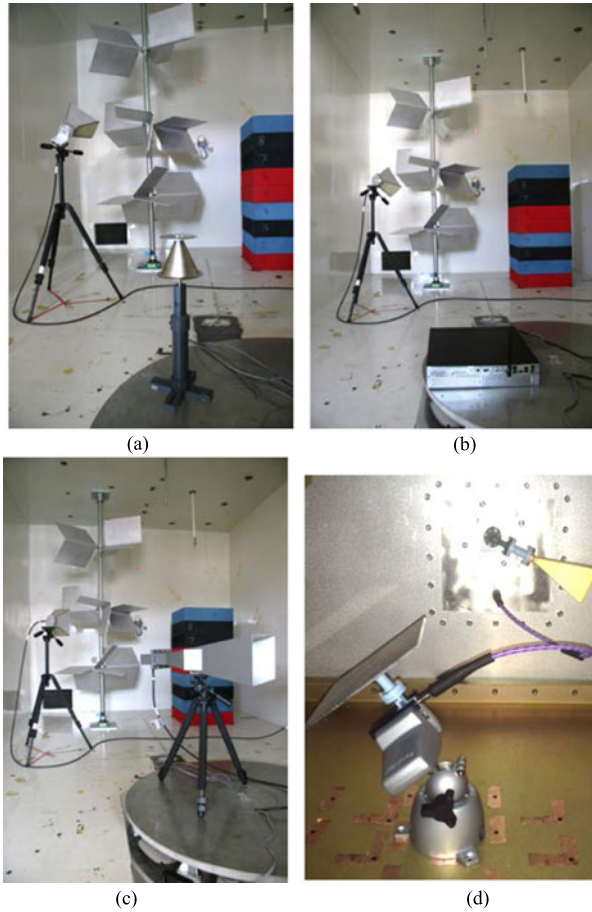


Fig. 2. Reverberation chamber measurement set-ups. In (a)–(c): microwave chamber with single rotating paddle and stack of RF absorber. At left is the 1–18 GHz dual-ridge-horn measurement antenna. (a) Discone omnidirectional reference antenna. (b) Router with omnidirectional reference antenna. (c) 2 GHz standard gain horn on turntable, cross polarized with the measurement antenna. (d) Millimeter-wave configuration with WR-22 horn measurement antenna and an open-ended waveguide with plate reference antenna. The plate allows surface currents to decay.

TABLE III
PARAMETERS OF THE VARIOUS ANTENNAS

	Antenna Type	Freq. Range (GHz)	Pattern (azimuth)	$\eta_{\text{rad, meas}}$	Ant. Gain (dBi)
Cellular and PCS bands	Discone	0.65–3.50	Omni	0.91	3.7
	Router	0.70–2.70	Omni	0.88	2
	Dual-Ridge Horn	0.75–18.0	Dir	0.92	≈ 4.5
	Standard Gain Horn	1.70–2.60	Dir	0.90	14.5
mmWave band	OEG + Plate	33.0–50.0	Omni halfspace	1	4.1
	Horn	33.0–50.0	Dir	0.97	22.1
	Patch	43.0–45.0	Omni halfspace	0.89	6.8

3 dB beamwidth was quite wide at our frequencies, contributing to significant direct coupling for some positions. Thus, the randomly polarized case resulted in a value of κ_R approaching or even exceeding that of the omnidirectional antennas.

For the “lower” K -factor configurations, we maintained strict cross-polarization between directional reference and

measurement antennas, with the two pointed away from each other for each of the nine antenna positions. These cases are represented by a cross-polarized reference antenna (termed “DRHA XPol”) and, for the PCS band, a 2 GHz standard gain horn (termed “Std Gain”), as shown in Fig. 2(c).

The three mmWave configurations all resulted in very low K factors because the chamber was unloaded and electrically large, and because the measurements were made at antenna positions that were optimized to minimize direct coupling. An open-ended waveguide with a metal plate to reduce radiation of surface currents from discontinuous edges (termed “OEG+PI”) [24] is shown in Fig. 2(d). We also used the same type of WR-22 waveguide horn antenna as the measurement antenna and a microstrip patch antenna fabricated at the Brigham Young University. The patch size was 1.26 mm \times 1.26 mm, and the ground size was 8 mm \times 8 mm. A textured metal sheet on the chamber’s wall reduced specular reflections into the measurement antenna, further reducing the K factor [24].

C. Measured Power Transfer Function and K Factor

We next compare measured values of G_{Ref} , $\sigma_{G_{\text{Ref}}}$, and κ_R for the configurations used in our study. Results are shown in Table IV for two loading conditions in the PCS (1.8–1.95 GHz) band, with similar results found for the Cellular band (not shown). The loading conditions consisted of an unloaded chamber and a chamber loaded with seven RF absorber blocks to provide a coherence bandwidth of approximately 3.85 MHz. The loading for the mmWave band results (43.0–47.0 GHz) resulted in a coherence bandwidth of approximately 10 MHz. Repeat measurements are not yet available for the loaded mmWave configuration.

As expected, the values of κ_R for the loaded cases are higher than those for the unloaded cases: for the PCS band, κ_R is around 5 dB higher as compared to the unloaded case. This effect was also seen for the Cellular band.

In addition to differences in κ_R due to loading, Table IV illustrates that κ_R may be substantially different depending on the antenna configuration. For the PCS band, κ_R varies as a function of antenna configuration by up to ~ 3 dB for the unloaded

TABLE IV
 G_{Ref} , $\sigma_{G_{\text{Ref}}}$, AND K FACTOR VALUES FOR CHAMBER CONFIGURATIONS UTILIZING VARIOUS REFERENCE ANTENNA TYPES AND FREQUENCY BANDS

	Antenna Type	G_{Ref} (dB)	$\sigma_{G_{\text{Ref}}}$ (dB)	κ_R (dB)	G_{Ref} (dB)	$\sigma_{G_{\text{Ref}}}$ (dB)	κ_R (dB)
		unloaded	unloaded	unloaded	loaded	loaded	loaded
PCS band	Discone	−23.07	0.21	−10.10	−29.88	0.38	−4.99
	Router	−23.07	0.19	−10.90	−29.98	0.34	−5.36
	DRHA (RPol)	−23.14	0.21	−9.98	−29.51	0.38	−4.31
	DRHA (XPol)	−23.37	0.04	−12.07	−30.64	0.17	−7.26
	Std Gain	−23.26	0.21	−12.95	−30.77	0.25	−8.66
mmWave band	OEG+PI	−36.20	0.02	−23.03	−48.99	TBD	−15.13
	Horn	−35.96	0.02	−28.25	−48.56	TBD	−21.38
	Patch	−35.67	0.02	−22.35	−48.85	TBD	−15.81

case and up to ~ 4.3 dB for the loaded case. For the mmWave measurements, the value of κ_R changed by up to ~ 6 dB depending on the antenna configuration. This illustrates clearly that the antenna type and orientation can have a strong influence on the unstirred fields.

IV. ERRORS ESTIMATING G_{DUT} DUE TO UNKNOWN K FACTOR

A. Measured Results

To study the impact of unknown K factor values on the estimate of G_{DUT} , we assessed the difference between measured values of G_{Ref} and G_{DUT} . Our goal is twofold: first to determine under what conditions an antenna introducing an unknown K factor may introduce a significant error in the assumption that $G_{\text{DUT}} = G_{\text{Ref}}$, and, second, to determine whether the correction from (15) can improve the estimate of G_{DUT} .

We designate one of the antennas described in Table III as the reference antenna and sequentially designate each of the other antennas as a simulated DUT antenna. Because we have access to the ports of the various antennas, we are able to estimate the “actual” values of both G_{Ref} and G_{DUT} . Thus, we can directly compare reference/DUT pairs introducing similar K factors to those introducing substantially different K factors. For each case, the measurement antenna is held constant. We may also then determine whether the correction factor significantly improves the estimate of G_{DUT} for each of the antenna pairs. In practice, it is often impossible to perform such comparisons because antennas are integrated into the DUT.

We define $G_{\text{DUT, Actual}}$ as the estimate of G_{DUT} derived from measurement of the chamber set-up’s transfer function for each simulated DUT antenna. We define $G_{\text{DUT, Pred}}$ as the estimate of G_{DUT} derived by applying the correction from (15) to G_{Ref} .

For the simple assumption that $G_{\text{DUT}} = G_{\text{Ref}}$, we define the error metric as

$$\Delta G_{\text{DUT}} = |G_{\text{DUT, Actual}} - G_{\text{Ref}}| \text{ dB}. \quad (17a)$$

For the case where the correction factor has been applied to predict G_{DUT} , our error metric is defined as

$$\Delta G_{\text{Pred}} = |G_{\text{DUT, Actual}} - G_{\text{DUT, Pred}}| \text{ dB}. \quad (17b)$$

The standard uncertainty associated with ΔG_{DUT} and ΔG_{Pred} is computed from the relation

$$u^2(X - Y) = u^2(X) + u^2(Y). \quad (18)$$

Thus,

$$u_{\Delta G_{\text{DUT}}}^2 = u_{G_{\text{DUT, Actual}}}^2 + u_{G_{\text{Ref}}}^2 \quad (19a)$$

and

$$u_{\Delta G_{\text{Pred}}}^2 = u_{G_{\text{DUT, Actual}}}^2 + u_{G_{\text{DUT, Pred}}}^2. \quad (19b)$$

Expanded uncertainty may be found as in (5). We calculated the standard uncertainty from the $N_B = 9$ measurements defined above. Note that the uncertainty in the estimate of κ was small enough to be neglected, so $u_{\Delta G_{\text{DUT}}}^2 = u_{\Delta G_{\text{Pred}}}^2$ for the

results shown here. The decibel representation is given by

$$u(10\log_{10}(\Delta G_{\text{DUT}})) \approx 10\log_{10}\left(\frac{G_{\text{Ref}} + u(\Delta G_{\text{DUT}})}{G_{\text{Ref}}}\right) \quad (20a)$$

$$u(10\log_{10}(\Delta G_{\text{Pred}})) \approx 10\log_{10}\left(\frac{G_{\text{DUT, Pred}} + u(\Delta G_{\text{Pred}})}{G_{\text{DUT, Pred}}}\right) \quad (20b)$$

where the mean associated with each estimate (G_{Ref} or $G_{\text{DUT, Pred}}$) was effectively subtracted by virtue of its position in the denominator.

The metrics from (17) and error bars from (19) and (20) are plotted in Fig. 3(a)–(c), where ΔG_{DUT} is plotted with Xs and ΔG_{Pred} is plotted with circles. The x -axis labels indicate the various simulated DUT antennas. In each figure, two different loading cases are shown: zero absorber (corresponding to a PCS-band coherence bandwidth of ~ 0.64 MHz for a threshold of 0.5) in black, and seven absorbers (corresponding to a coherence bandwidth of ~ 3.5 MHz) in red.

In Fig. 3(a) and (b), the reference antenna was omnidirectional (the discone for the microwave bands and the open-ended waveguide for the mmWave bands), providing a low- K -factor environment. In Fig. 3(c), the reference antenna was highly directional (the PCS-band standard gain horn), providing a high- K -factor environment. The frequency bands are labeled in the graphs.

For the unloaded chamber (data plotted in black), the circles (ΔG_{Pred}) and the Xs (ΔG_{DUT}) are in close proximity to each other and are also close to zero. This indicates that G_{Ref} provides a reasonable estimate of G_{DUT} and that the use of the correction factor does not significantly improve the estimate of G_{DUT} . In fact, ΔG_{Pred} would not be significantly different from ΔG_{DUT} even at the 90% confidence interval (defined in Table I).

The low values of ΔG_{DUT} and ΔG_{Pred} for the unloaded chamber are expected because the stirred energy dominates and, as mentioned in Section I, reverberation-chamber measurements in unloaded chambers have the effect of eliminating antenna pattern [16]. Ideally, energy arrives at the measurement antenna (minus the chamber loss) no matter the direction in which it was launched, assuming antennas are not oriented toward each other or copolarized.

For the loaded chamber, the red Xs (ΔG_{DUT}) corresponding to the assumption that $G_{\text{DUT}} = G_{\text{Ref}}$ indicate low error in an estimation of G_{DUT} when the reference antenna is of a “similar” type as the DUT. This is shown in Fig. 3(a) and (b) for the PCS and Cellular bands, where the omnidirectional reference antenna is used to estimate G_{DUT} for the omni-like router (point 1) and the randomly polarized horn antenna (point 2), and in Fig. 3(c) when the directional standard gain horn reference antenna is used to estimate G_{DUT} for the directional cross-polarized horn antenna (point 4). For these cases of similar antennas, the overlap of the error bars associated with the circles (ΔG_{Pred}) and the Xs (ΔG_{DUT}) indicates that the use of the correction factor would not significantly improve the estimate of G_{DUT} .

However, when the value of κ associated with the DUT antenna differs significantly from that of the reference antenna,

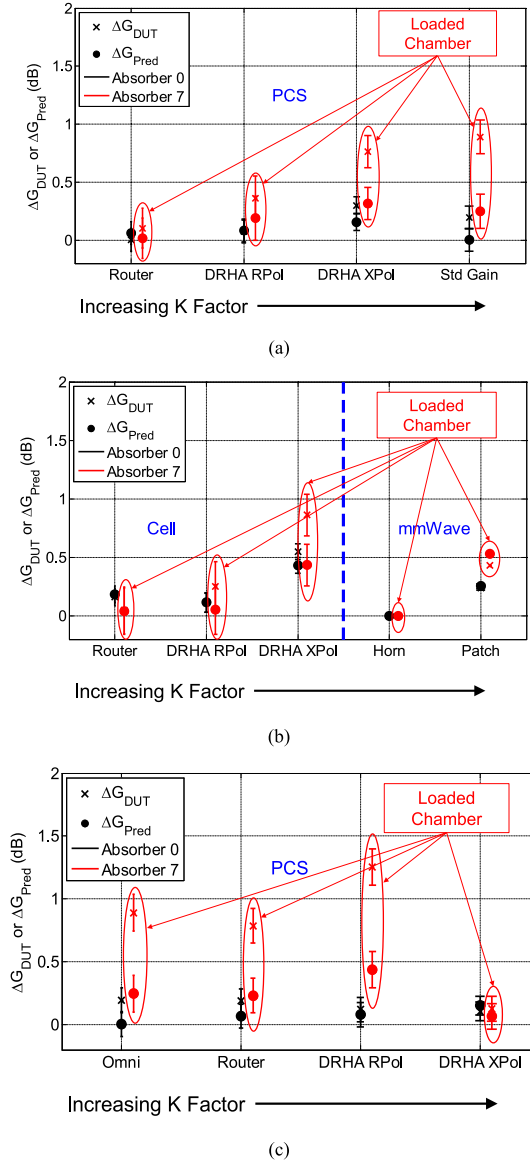


Fig. 3. Difference between the measured power transfer function $G_{\text{DUT, Actual}}$ and the power transfer function approximated as either $G_{\text{DUT}} = G_{\text{Ref}}$ (ΔG_{DUT}) or $G_{\text{DUT}} = G_{\text{DUT, Pred}}$ from (15) (ΔG_{Pred}). 0 dB corresponds to the case where there is no error in the estimate of G_{DUT} . Various simulated DUT antennas are denoted along the x axis. In (a) and (b), the reference antenna is omnidirectional and in (c), the reference antenna is a highly directional standard gain horn. Error bars correspond to $\pm u_{\Delta G_{\text{DUT}}}$ or $u_{\Delta G_{\text{Pred}}}$ defined in (20).

the error bars for the red circles (ΔG_{Pred}) and Xs (ΔG_{DUT}) do not overlap, indicating that G_{Ref} provides a poorer estimate of G_{DUT} . This effect is illustrated in Fig. 3(a) and (b) when the omnidirectional reference antenna is used to predict G_{DUT} of the directional DUT antennas “DRHA XPol” (point 3) and “Std Gain” horn (point 4) antennas. The poorer estimate of G_{DUT} is also seen in Fig. 3(c) when the directional standard gain horn reference antenna is used to predict G_{DUT} for the omnidirectional and effectively omnidirectional antennas “omni,” “router,” and “DRHA Rand Pol” (points 1–3).

For the cases where G_{Ref} provides a relatively poor estimate of G_{DUT} , application of the correction factor provides

an improvement. The only case where a statistically significant improvement is seen for the omnidirectional reference antenna is when paired with the standard gain horn DUT antenna in Fig. 3(a). This case shows an improvement in the estimate of G_{DUT} at the 95% confidence level. For the other cases in Fig. 3(a) and (b), the improvement is not significant even at the 90% confidence level. For the directional standard gain horn reference antenna, the improvement is significant at the 95% confidence level for the “router” antenna in Fig. 3(c), increasing to 99% for “omni” and “DRHA Rand Pol” cases. Thus, the use of a directional reference antenna to estimate G_{DUT} may significantly benefit from the use of (15). Note that for all of the cases presented in Fig. 3, the maximum error is less than 1.5 dB, which occurs with the standard gain horn directional reference and omnidirectional DUT antenna pair.

As illustrated, the differences between G_{Ref} and G_{DUT} due to different configuration K factors occur under loaded conditions when waves interact with the absorber before reaching the measurement antenna. This interaction can be expected to occur more for omnidirectional antennas (and poorly oriented directional antennas) as compared to directional antennas oriented away from and cross-polarized to each other. This motivates use of the correction factor when one type (omnidirectional or directional) is used to estimate G_{DUT} for the other type.

To summarize, for the cases studied here: 1) For unloaded chambers, low- κ cases, and cases where antennas introduce “similar” values of κ into a given chamber set-up, the estimate of G_{DUT} provided by G_{Ref} is not statistically different from that provided by use of the correction factor to the 90% confidence level. 2) When the reference antenna-created κ is “quite different” from that created by the DUT antenna, the correction from (15) may provide a statistically significant improvement.

B. Use of Correction Factor to Bound Error

The antenna configurations presented above exemplify “typical” set-ups currently used for testing cellular devices in reverberation chambers in terms of

- 1) antenna types (from omnidirectional to cross-polarized directional);
- 2) chamber loading conditions (from unloaded to heavily loaded); and
- 3) lack of spatial uniformity (a heavily loaded, large chamber with many modes, causing relatively high peaks and nulls in the average fields within the chamber).

It would be possible to find set-ups that exceed these bounds, such as the use of an omnidirectional antenna to estimate G_{DUT} for a highly directional “pencil-beam” antenna. We can extend the range of possible K factors with a simulation study.

We define ΔG_x as the difference between $G_{\text{Ref}, x}$ and $G_{\text{DUT, Pred}}$, which is given by the correction factor from (15), for various simulated values of κ_{D} . For this study, reference antenna x is either the omnidirectional disccone or the standard gain horn, and we use the values of κ_{R} associated with those antennas (approximately -5 dB for the disccone set-up and -8.7 dB for the standard gain horn set-up) in (15). We allow the simulated κ_{D} to vary both below (to -30 dB) and above (to -3 dB) the measured κ_{R} .

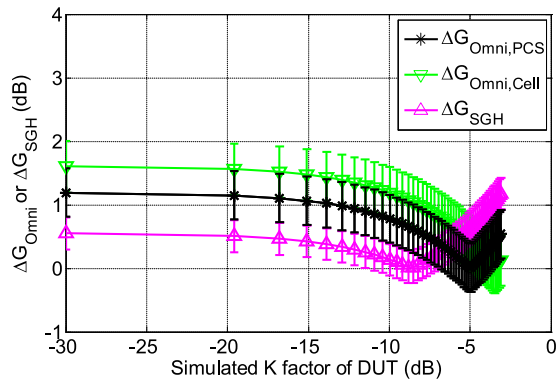


Fig. 4. Simulation study illustrating the impact on G_{DUT} for an extended range of κ_{DUT} values. ΔG_x denotes the difference between $G_{Ref,x}$ and $G_{DUT,pred}$, where x corresponds to the omnidirectional disc (omni) or standard gain horn (SGH) reference antenna.

Fig. 4 plots ΔG_x for $x = \text{omni}$ and $x = \text{standard gain horn}$. Both PCS and Cellular band frequencies are plotted for the omnidirectional reference antenna, and the PCS band results for the standard gain horn reference antenna. The error bars correspond to $\pm\sigma_{G_{Ref}}$ for the selected reference antenna (see Table IV). The points in the simulation corresponding to the measured values of G_{Ref} , κ_R , and κ_D are shown by the minima in each plot.

Fig. 4 shows that for cases where the DUT antenna is more directional than the reference antenna, corresponding to lower values of κ_D , the error reaches a plateau beyond which there is little change. This error is most significant for the omnidirectional reference antenna in the Cellular band. For cases where the DUT antenna is less directional than the reference antenna (to the right of the minima in Fig. 4), the error increases. For our set-up, the errors can be 2 dB or more, depending on the antenna configurations used, motivating the use of the correction factor when possible.

By performing measurements with typical antenna types in a given reverberation chamber set-up, and then extending the range of the DUT's K -factor by plotting the correction factor, individual users should be able to estimate the extent of the error in G_{DUT} when measuring devices that introduce unknown K factors. This could provide an uncertainty element in a standardized test procedure or provide a limit on the range of acceptable DUT antenna types to be tested.

V. CONCLUSION

We studied potential errors in reverberation-chamber measurements of wireless devices arising from the simple assumption that $G_{DUT} = G_{Ref}$ when the K factor introduced by the DUT antenna is significantly different from that of the reference antenna. For both unloaded and loaded chambers, this work indicates that an omnidirectional reference antenna approximates an omnidirectional DUT antenna quite well and a well-oriented directional reference antenna approximates a well-oriented DUT antenna well.

In unloaded chambers, little effect was seen on the estimate of the DUT's transfer function, even when the DUT antenna

radiation pattern is quite different from that of the reference antenna, such as when an omnidirectional reference antenna is used but the DUT has a highly directional antenna.

However, for loaded chambers, the error can be statistically significant. When radiation patterns of the DUT and reference antennas are different, a correction factor can improve the estimate of the chamber's transfer function. We illustrated conditions where the correction factor would provide a statistically significant improvement and derived a method that could be used to extend the range of antenna types for these cases.

The results presented here were intended to represent "typical" conditions used in current OTA test. As antennas in future 5G wireless system are expected to become more and more directional, the role of the unknown K factor in device measurements may soon become more significant.

ACKNOWLEDGMENT

The authors are grateful to Z. Yang and K. F. Warnick in the Department of Electrical and Computer Engineering, Brigham Young University, Provo, UT 84602 USA, for providing the microstrip patch antenna.

REFERENCES

- [1] P.-S. Kildal, C. Orlenius, and J. Carlsson, "OTA testing in multipath of antennas and wireless devices with MIMO and OFDM," *Proc. IEEE*, vol. 100, no. 7, pp. 2145–2157, Jul. 2012.
- [2] C. L. Patané, A. Skårbratt, R. Rehammar, and C. Orlenius, "On the use of reverberation chambers for assessment of MIMO OTA performance of wireless devices," in *Proc. 7th Eur. Conf. Antennas Propag.*, Gothenburg, Sweden, 2013, pp. 101–105.
- [3] 3rd Generation Partnership Project, "Technical specification group radio access networks; universal terrestrial radio access (UTRA) and evolved universal terrestrial radio access (E-UTRA); Verification of radiated multi-antenna reception performance of user equipment (UE)," rel. 12, 3GPP TR 37.977 v1.3.0, Nov. 2013.
- [4] D. Micheli, M. Barazzetta, F. Moglie, and V. M. Primiani, "Power boosting and compensation during OTA testing of a real 4G LTE base station in reverberation chamber," *IEEE Trans. Electromagn. Compat.*, vol. 57, no. 4, pp. 623–634, Aug. 2015.
- [5] CTIA Certification, "Test plan for wireless large-form-factor device over-the-air performance," v. 1.0.1, Oct. 2016.
- [6] X. Chen, P.-S. Kildal, C. Orlenius, and J. Carlsson, "Channel sounding of loaded reverberation chamber for over-the-air testing of wireless devices - coherence bandwidth versus average mode bandwidth and delay spread," *IEEE Antennas Wireless Propag. Lett.*, vol. 8, pp. 678–681, 2009.
- [7] K. A. Remley, S. J. Floris, H. A. Shah, and C. L. Holloway, "Static and dynamic propagation-channel impairments in reverberation chambers," *IEEE Trans. Electromagn. Compat.*, vol. 53, no. 3, pp. 589–599, Aug. 2011.
- [8] K. A. Remley *et al.*, "Configuring and verifying reverberation chambers for testing cellular wireless devices," *IEEE Trans. Electromagn. Compat.*, vol. 58, no. 3, pp. 661–672, Jun. 2016.
- [9] A. Goldsmith, *Wireless Communications*. Cambridge, U.K.: Cambridge Univ. Press, 2005.
- [10] P. Corona, G. Ferrara, and M. Migliaccio, "Reverberating chamber electromagnetic field in presence of an unstirred component," *IEEE Trans. Electromagn. Compat.*, vol. 42, no. 2, pp. 111–115, May 2000.
- [11] Joint Task Force IEC SC77B-CISPR/A, "Electromagnetic compatibility (EMC)—Part 4.21: Testing and measurement techniques—Reverberation chamber test methods," IEC 61000-4-21, Geneva, Switzerland, Aug. 2003.
- [12] R. J. Pirkl, J. M. Ladbury, and K. A. Remley, "The reverberation chamber's unstirred field: A validation of the image theory interpretation," in *Proc. Int. Symp. Electromagn. Compat.*, Long Beach, CA, USA, Aug. 2011, pp. 670–675.

- [13] P.-S. Kildal, X. Chen, C. Orlenius, M. Franzen, and C. L. Patané, "Characterization of reverberation chambers for OTA measurements of wireless devices: physical formulations of channel matrix and new uncertainty formula," *IEEE Trans. Antennas Propag.*, vol. 60, no. 8, pp. 3875–3891, Aug. 2012.
- [14] K. A. Remley, R. J. Pirkl, H. A. Shah, and C.-M. Wang, "Uncertainty from choice of mode-stirring technique in reverberation-chamber measurements," *IEEE Trans. Electromagn. Compat.*, vol. 55, no. 6, pp. 1022–1030, Dec. 2013.
- [15] X. Chen and P.-S. Kildal, "Frequency-dependent effects of platform and wall antennas on measurement uncertainty in reverberation chamber," in *Proc. 5th Eur. Conf. Antennas Propag.*, Barcelona, Spain, 2010, pp. 1–3.
- [16] D. A. Hill, *Electromagnetic Fields in Cavities: Deterministic and Statistical Theories*. Piscataway, NJ, USA: Wiley, 2009.
- [17] W. T. C. Burger, C. L. Holloway, and K. A. Remley, "Proximity and orientation influence on Q-factor with respect to large-form-factor loads in a reverberation chamber," in *Proc. 2013 Int. Symp. Electromagn. Compat.*, Brugge, Belgium, Sep. 2013, pp. 369–374.
- [18] J. A. D. Toorn, K. A. Remley, C. L. Holloway, J. M. Ladbury, and C.-M. Wang, "Proximity-effect test for lossy wireless-device measurements in reverberation chambers," *IET Sci., Meas., Technol.*, vol. 9, no. 5, pp. 540–546, 2015.
- [19] K. A. Remley *et al.*, "A significance test for reverberation-chamber measurement uncertainty in total radiated power of wireless devices," *IEEE Trans. Electromagn. Compat.*, vol. 58, no. 1, pp. 207–219, Oct. 2015.
- [20] C. L. Holloway, H. A. Shah, R. J. Pirkl, W. F. Young, D. A. Hill, and J. Ladbury, "Reverberation chamber techniques for determining the radiation and total efficiency of antennas," *IEEE Trans. Antennas Propag.*, vol. 60, no. 4, pp. 1758–1770, Apr. 2012.
- [21] Joint Committee for Guides in Metrology, "Evaluation of measurement data—Guide to the expression of uncertainty in measurement," Int. Bureau Weights Measures, S'evres, France, Sep. 2008. [Online]. Available: <http://www.bipm.org/en/publications/guides/gum.html>
- [22] C. L. Holloway, D. A. Hill, J. M. Ladbury, P. F. Wilson, G. Koepke, and J. Coder, "On the use of reverberation chambers to simulate a Rician radio environment for the testing of wireless devices," *IEEE Trans. Antennas Propag.*, vol. 54, no. 11, pp. 3167–3177, Nov. 2006.
- [23] X. Chen, P.-S. Kildal, and S.-H. Lai, "Estimation of average Rician K-factor and average mode bandwidth in loaded reverberation chamber," *IEEE Antennas Wireless Propag. Lett.*, vol. 10, pp. 1437–1440, 2011.
- [24] D. Senic *et al.*, "Improved antenna efficiency measurement uncertainty in a reverberation chamber at millimeter-wave frequencies," *IEEE Trans. Antennas Propag.*, 2017, vol. 65, no. 8, Aug. 2017.



Kate A. Remley (S'92–M'99–SM'06–F'13) was born in Ann Arbor, MI, USA. She received the Ph.D. degree in electrical and computer engineering from the Oregon State University, Corvallis, OR, USA, in 1999.

From 1983 to 1992, she was a Broadcast Engineer in Eugene, OR, serving as a Chief Engineer of an AM/FM broadcast station from 1989 to 1991. In 1999, she joined the RF Technology Division, National Institute of Standards and Technology (NIST), Boulder, CO, USA, as an Electronics Engineer. She

is currently the Leader of the Metrology for Wireless Systems Group, NIST, where her research interests include development of calibrated measurements for microwave and millimeter-wave wireless systems, characterizing the link between nonlinear circuits and system performance, and developing standardized test methods for the wireless industry.

Dr. Remley is a member of the Oregon State University Academy of Distinguished Engineers. She was the Chair of the MTT-11 Technical Committee on Microwave Measurements from 2008 to 2010 and the Editor-in-Chief of *IEEE Microwave Magazine* from 2009 to 2011, and is the Chair of the MTT Fellow Evaluating Committee. She is a Distinguished Lecturer for the IEEE Electromagnetic Compatibility Society (2016–2017). She received the Department of Commerce Bronze and Silver Medals and an ARFTG Best Paper Award.



Ryan J. Pirkl (S'06–M'10) received the B.S., M.S., and Ph.D. degrees in electrical engineering from the Georgia Institute of Technology, Atlanta, GA, USA, in 2005, 2007, and 2010, respectively. For his graduate research, he developed hardware, measurement procedures, and processing tools for *in situ* characterization of radio wave propagation mechanisms.

In 2010, he began working with the National Institute of Standards and Technology, Boulder, CO, USA, under a National Research Council Postdoctoral Research Associateship. There, he investigated how reverberation chambers may be used as tunable wireless channel emulators for wireless device testing. In 2012, he joined the Subscriber Product Engineering team at AT&T Mobility. In 2014, he joined the Signal and Information Sciences Laboratory, University of Texas Applied Research Laboratories. His research interests include reverberation chambers, wave propagation, analytical electromagnetics, sonar, and signal processing.



Chih-Ming Wang received the Ph.D. degree in statistics from Colorado State University, Fort Collins, in 1978. Since 1988, he has been with the Statistical Engineering Division, National Institute of Standards and Technology, Boulder, CO. He has published over 90 journal articles. His research interests include statistical metrology and the application of statistical methods to physical sciences.

Dr. Wang is a fellow of the American Statistical Association (ASA). He is the recipient of the Department of Commerce Silver Medal, Bronze Medal, the

NIST Allen V. Astin Measurement Science Award, and several awards from ASA.



Damir Senić (S'09–M'16) received the M.Sc. degree in 2008 and Ph.D. degree in radio communication in 2014 both from the Faculty of Electrical Engineering, Mechanical Engineering and Naval Architecture, University of Split, Split, Croatia.

He is currently with the University of Colorado Boulder and the National Institute of Standards and Technology, Boulder, CO, USA, as a Postdoctoral Research Associate through Professional Research Experience Program. From 2013 to 2014, he was a Guest Researcher with the National Institute of Standards and Technology, where he

worked on human exposure and wireless communications aspects of electromagnetic wave absorption in dissipative objects inside reverberant environment. His research interests include millimeter wave radiocommunications, over-the-air measurements in reverberation chambers at millimeter wave and microwave frequencies, electromagnetic compatibility, and bioeffects of EM fields.

Dr. Senić received the Richard E. Merwin Award of the IEEE Computer Society for exemplary involvement in IEEE activities and excellent academic achievement in 2013. In 2016, he was elected as a Distinguished Reviewer of the IEEE TRANSACTIONS ON ELECTROMAGNETIC COMPATIBILITY.

Arvand C. Homer is currently working toward B.S. degree in electrical engineering in the Department of Electrical and Computer Engineering, University of Maryland, College Park, MD, USA. His expected graduation date is December 2018.

He interned in the Communications Technology Laboratory, National Institute of Standards and Technology, Boulder, CO, USA, in the summer of 2016 through the Summer Undergraduate Research Fellowship program. There, he performed over-the-air testing on a range of antenna types and for multiple

loading conditions to verify the power transfer function approximation. He is currently working in the Flight Microwave and Telecommunication Systems Branch, NASA Goddard Space Flight Center, Greenbelt, MD, USA, as a co-op student through the Pathways program. He is developing an end-to-end simulation of M-PSK modulation techniques over an additive white Gaussian noise channel.

Matt V. North, photograph and biography not available at the time of publication.



Maria G. Becker received the B.S., M.S., and Ph.D. degrees in physics from the University of Nebraska-Lincoln, Lincoln, NE, Nebraska, USA, in 2010, 2013, and 2016, respectively. Her graduate research involved ultrafast free electron quantum optics.

In 2016, she joined as a National Research Council Postdoctoral Research Associate the Communications Technology Laboratory, National Institute of Standards and Technology, Boulder, CO, USA, where she is investigating the use of reverberation chambers for wireless device metrology. Her current re-

search interests include reverberation chambers, analytical electromagnetics, and millimeter-wave wireless metrology.



Robert D. Horansky (M'15) received the B.A. degree in chemistry and the Ph.D. degree in physics from the University of Colorado at Boulder, Boulder, CO, USA, in 1999 and 2005, respectively. His thesis work focused on low-noise dielectric measurements on novel materials.

Since 2005, he has been with the National Institute of Standards and Technology (NIST), Boulder, CO, USA, where he started out developing the highest resolving power energy dispersive sensor to date. He then went on to develop metrology techniques for

single photon sensors in nuclear radiation and optical power measurements. In 2015, he joined the Metrology for Wireless Systems Group in the Communication Technology Laboratory, NIST developing calibrations and traceability for millimeter-wave wireless systems and reverberation-chamber measurements for cellular applications.

Dr. Horansky serves as a Secretary of the IEEE P1765 Standards Working Group on uncertainty for EVM and other wireless metrics.



Christopher L. Holloway (S'86–M'92–SM'04–F'10) received the B.S. degree in engineering from the University of Tennessee at Chattanooga, Chattanooga, TN, USA, in 1986 and the M.S. and Ph.D. degrees in electrical engineering from the University of Colorado at Boulder, Boulder, CO, USA, in 1989 and 1992, respectively.

During 1992, he was a Research Scientist with Electro Magnetic Applications, Inc., Lakewood, CO. His responsibilities included theoretical analysis and finite-difference time-domain modeling of various electromagnetic problems. From the fall of 1992–1994, he was with the National Center for Atmospheric Research (NCAR), Boulder, CO. While with NCAR his duties included wave propagation modeling, signal processing studies, and radar systems design. From 1994 to 2000, he was in the Institute for Telecommunication Sciences, U.S. Department of Commerce, Boulder, CO, where he was involved in wave propagation studies. Since 2000, he has been with the National Institute of Standards and Technology (NIST), Boulder, CO, USA, where he works on electromagnetic theory. He is also on the Graduate Faculty, University of Colorado at Boulder, Boulder, CO, USA. His research interests include electromagnetic field theory, wave propagation, guided wave structures, remote sensing, numerical methods, metamaterials, measurement techniques, electromagnetic compatibility/interference issues, and atom-based metrology.

Dr. Holloway is a member of URSI Commissions A, B, and E. He served as the Chair for US Commission A of the International Union of Radio Science from 2012 to 2015, and is currently an Associate Editor for the IEEE TRANSACTIONS ON ELECTROMAGNETIC COMPATIBILITY. He was the Chairman for the Technical Committee on Computational Electromagnetics (TC-9) of the IEEE Electromagnetic Compatibility Society from 2000 to 2005, served as the Co-Chair for the Technical Committee on Nano-Technology and Advanced Materials (TC-11) of the IEEE EMC Society from 2006 to 2011, and served as an IEEE Distinguished Lecturer for the EMC Society from 2004 to 2006.